J. Phys.: Condens. Matter **21** (2009) 025904 (13pp) doi:10.1088/0953-8984/21/2/025904

Dispersive dielectric and conductive effects in 2D resistor–capacitor networks

R F Hamou[1], J R Macdonald[2] and E Tuncer[3]

[1] Max-Planck-Institut für Eisenforschung GmbH, Max-Planck-Straße 1, 40237 Düsseldorf, Germany
[2] Department of Physics and Astronomy, University of North Carolina, Chapel Hill, NC 27599-3255, USA
[3] Applied Superconductivity Group, Fusion Energy Division, Oak Ridge National Laboratory, Oak Ridge, TN 37831-6122, USA

Received 12 April 2008, in final form 29 September 2008
Published 11 December 2008
Online at stacks.iop.org/JPhysCM/21/025904

Abstract
How to predict and better understand the effective properties of disordered material mixtures has been a long-standing problem in different research fields, especially in condensed matter physics. In order to address this subject and achieve a better understanding of the frequency-dependent properties of these systems, a large 2D $L \times L$ square structure of resistors and capacitors was used to calculate the immittance response of a network formed by random filling of binary conductor/insulator phases with 1000 Ω resistors and 10 nF capacitors. The effects of percolating clusters on the immittance response were studied statistically through the generation of 10 000 different random network samples at the percolation threshold. The scattering of the imaginary part of the immittance near the dc limit shows a clear separation between the responses of percolating and non-percolating samples, with the gap between their distributions dependent on both network size and applied frequency. These results could be used to monitor connectivity in composite materials. The effects of the content and structure of the percolating path on the nature of the observed dispersion were investigated, with special attention paid to the geometrical fractal concept of the backbone and its influence on the behavior of relaxation-time distributions. For three different resistor–capacitor proportions, the appropriateness of many fitting models was investigated for modeling and analyzing individual resistor–capacitor network dispersed frequency responses using complex-nonlinear-least-squares fitting. Several remarkable new features were identified, including a useful duality relationship and the need for composite fitting models rather than either a simple power law or a single Davidson–Cole one. Good fits of data for fully percolating random networks required two dispersive fitting models in parallel or series, with a cutoff at short times of the distribution of relaxation times of one of them. In addition, such fits surprisingly led to cutoff parameters, including a primitive relaxation or crossover time, with estimated values comparable to those found for real dispersive materials.

1. Background and introduction

Electrical and optical properties of disordered systems have been the focus of both theoretical and practical work [1–3]. Disordered, inhomogeneous structures have physical properties determined by the properties of the constituents and the microstructure or microgeometry of the composite system. Studies on the steady state properties of such systems have been performed in great detail [2, 4–9]. Little attention has been given, however, to the frequency-dependent properties of disordered systems [10–12]. In regular/ordered and dilute mixtures (concentrations far away from a percolation threshold), the frequency-dependent dielectric response is expressed as a Debye-like relaxation [12]. But near percolation non-Debye dispersive responses are observed [10–12].

In nature, nearly all experimental frequency-response data for a wide variety of both dielectric and conductive materials exhibit dispersive response involving fractional power-law (FPL) dependence over appreciable frequency

ranges. Such dispersive behavior has often been characterized as 'universal dielectric response' or, more generally, as 'universal dynamic response'. Reference [13] provides a detailed discussion of its provenance and of its limited applicability as a general fitting model. More generally, [14] divides theoretical data interpretations into three categories, 'relaxation-time distribution analysis, many-body effects on relaxation processes, and electrical network analysis'. The authors of [14] also emphasize the ubiquity of FPL and the need to account for its presence in the response of real materials.

Much valuable work investigating the behavior of two-dimensional (2D) networks of randomly positioned resistors and capacitors (RC) appears in [10] and [14–16]. References to even earlier work on the subject are provided in [10]. Other relevant work dealing with FPL, effective-medium theories, and random binary composites appears in [2, 5, 8, 9, 11, 12] and [17–41]. In [14] it is pointed out that real conducting materials exhibiting microstructural heterogeneity involve a complex network of conduction paths and thus should behave as a bond-percolation network of conducting and capacitative regions, with consequent FPL response. An important 1974 paper on the bond theory of infinite clusters [42] shows the relation of this theory to hopping conduction. Disordered binary composites, conducting polymers, dielectrics, ion-conducting glasses, and random RC networks (RRCN) should therefore all exhibit FPL response and indeed do so. Most work using RRCN models has therefore emphasized their generation of limited-range FPL response at the cost of more detailed attention to full-range behavior and to deviations from FPL response. This lack is addressed by the results of the present work.

The number of nodes of a binary square network is given by $L \times L$, resulting in $2 \times L \times L$ total components for full occupancy. Define P as the number of capacitors and $(2 \times L \times L - P)$ as the number of resistors; thus $p \equiv P/2 \times L \times L$ is the capacitative fraction. We may then represent the percentage occupancy of a network as $100p$ and $100(1 - p)$, and for simplicity list it as either $100p/100(1-p)$ or $p\%C(1-p)\%R$. The percolation threshold value is $p = p_c = 0.5$. A diagram of a typical 10×10 network appears in [10]. Much of past RRCN work has been carried out with the $L = 16$ choice, but in [15] the effect of increasing L up to 128 has been investigated. Since some change in response still appears between this value and smaller ones, the present work involves comparison of results for $L = 128$, 256, and 500. For the $L = 500$ value, its number of 500 000 total components is thus more than 15 times larger than that for $L = 128$. Although 3D RRCN studies have been carried out (e.g., [2, 5c, 29]), the present work is restricted to the simpler 2D situation since the 3D studies 'are found to be qualitatively the same as those of 2D network simulations' [10].

Although critical phenomena (percolation behaviors) are similar for 2D and 3D systems, characteristic geometrical descriptions and electromagnetic interactions are different. The geometrical description can be understood by considering the nodes–links–blobs picture for a percolating network [42–44]. This model describes the percolating backbone by a multiple combination of nodes and links followed by a self-similar distribution of blob connections and dangling bonds along the chain. The model was successfully used to describe the change in the electric conductivity of a polymer composite during the mixing process [45]. The backbone within its multiple-blob connections behaves as a fractal object and thus has a fractal dimension. The disordered fractal structure has a dominant effect on the determination of the physical properties; this effect will be discussed in section 2.

Percolation in continuous binary mixtures was previously studied by solving Maxwell equations in the quasi-static limit [8, 32, 33]. In those simulations it was explicitly shown that, depending on the material parameters and geometrical description, different types of relaxations could be observed in mixtures [11, 12]. In a previous investigation, one of us studied all possible geometrical arrangements in a binary mixture with square tiles on a 4×4 lattice and showed the influence of the geometrical arrangement on the dielectric dispersion [34]. Here, a much larger scale is considered for RC network structures.

In [10, 16], the logarithmic mixing rule [36] is shown to lead for 2D RRCN situations to the FPL responses $\sigma(\omega) \propto (\mathrm{i}\omega)^p$ and $\varepsilon(\omega) \propto (\mathrm{i}\omega)^{p-1}$, where, as defined above, p is the proportion of the capacitative elements of the network. In the present work we make no distinction between original data sets and their specific form; thus σ' has the dimension of Siemens, sometimes written 'mho'. In the higher-frequency region where RRCN behavior is expected to be of FPL form, the mixing rule predicts that its fractional exponents, equal to the log–log slopes of the above responses, should be p and $-(1 - p)$ for $\sigma'(\omega)$ and $\varepsilon'(\omega)$, respectively. As we shall find, however, these results are only approximate when p differs appreciably from its critical $p = p_c \equiv 0.5$ percolation threshold value where a kind of metal–insulator transition occurs.

The main goal of this work is to explore how well the conductive and dielectric dispersive responses of random mixtures and other inhomogeneous real materials may be modeled by the RRCN approach. It is well known that a distribution-of-relaxation-times (DRT) approach and dispersive response models consistent with it may be successfully used to model both conductive and dielectric experimental data (e.g., [13, 37–41]). Central aims of the present work are to explore the statistical behavior of highly replicated, large RRCN models at the 50/50 percolation threshold, as well as the degree to which the frequency response of $p = 0.5$ and $p \neq 0.5$ models involves FPL behavior and may be well represented by dispersive models used in the past to best fit the response of disordered real materials. The statistical study is presented in section 2, and in section 3 and the appendix we discuss the results of an investigation carried out with complex-nonlinear-least-squares (CNLS) fitting of individual simulated RRCN data sets at and on either side of the percolation threshold.

2. Statistical investigation results for $p = p_c$

In this section we present numerical results for the immittance responses of highly replicated 2D RC-square networks. The

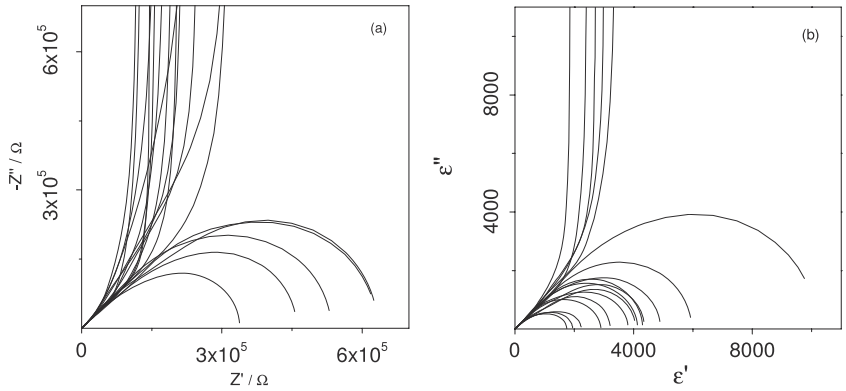

Figure 1. Complex-plane impedance and relative permittivity plots for 18 different RRCN samples at the 50/50 percolation threshold.

system, of maximum size 500 × 500, is composed of a random distribution of $R = 1000\ \Omega$ resistances and $C = 10$ nF capacitors with proportions equal to the 2D 50/50 percolation threshold. The immittance response for each replication of the network is calculated from 1 Hz to 1 GHz using the efficient Frank–Lobb reduction algorithm [30, 31]. The RRCN may be considered a bond percolating circuit structure and undergoes a metal–insulator transition at the percolation threshold where a percolating path between the electrodes may appear. The relation $\varepsilon(\omega) = \sigma(\omega)/(\mathrm{i}\omega\varepsilon_{\mathrm{V}})$ is used here for transformation between dielectric and admittance quantities, where ε_{V} is the permittivity of vacuum.

Figure 1 shows 18 different 2D 50/50 RRCN complex-plane responses that demonstrate remarkably well the transition from dominant conductive to dominant dielectric response. Either of these types are possible even for this percolation threshold choice because of the random placement of the equal numbers of resistors and capacitors of each network sample. Here the concave-arc lines of figure 1(a) involve conductive percolation-backbone response between the electrodes, while those of figure 1(b) are of dielectric percolation-backbone character. They both reach the x-axis at the right at zero frequency. The convex lines of figure 1(a) involve percolating dielectric behavior and those in figure 1(b) show percolating conductive behavior. As the figure shows, the 18 replication results exhibit appreciably different values of the percolating $\rho_0 \equiv 1/\sigma_0$ and ε_0 low-frequency-limiting values of $\rho'(\omega)$ ($Z'(\omega)$ in figure 1(a)) and $\varepsilon'(\omega)$: the relaxation strengths of the dispersions at the conductive and dielectric levels, respectively. Thus, a much larger replication number is needed to obtain statistically significant results.

In the dc limit, the phase exhibited by RRCN structures depends on the presence or absence of electrode-to-electrode backbones. In the absence of a backbone of either resistive or capacitative character and also in the presence of one or more capacitative backbones, the phase at the admittance level will be 90°, while in the presence of one or more resistive backbones, the phase will be zero. Because the present data extend only down to 1 Hz, we cannot expect exact dc results at this frequency, but the 1 Hz results are used here as approximate surrogates for actual dc ones.

Figures 2–5 present results at 1 Hz for 10 000 replications of RRCN structures of three different sizes at the percolation

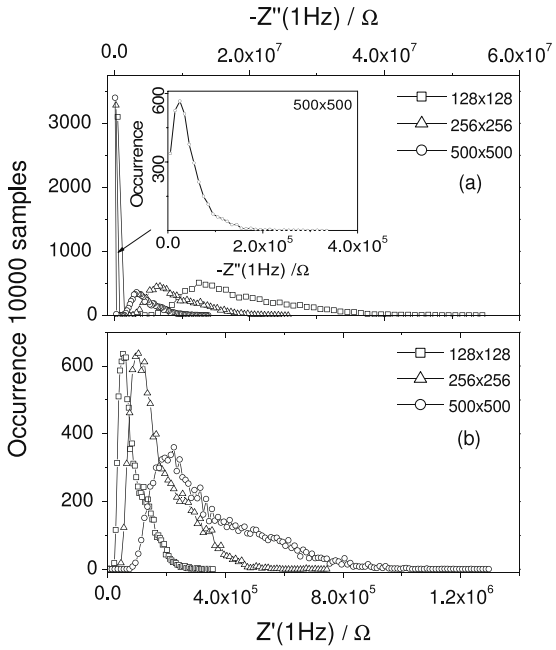

Figure 2. Distributions of $-Z''(1\ \mathrm{Hz})$ and $Z'(1\ \mathrm{Hz})$ responses for 10^4 50/50 samples and three different network sizes.

threshold. Note the appreciable size effects, especially near the zero-frequency limits. For the real part of the impedance, figure 2(b) shows that approximate log-normal distributions are evident, ones whose widths increase with the size of the network. In the dc limit the values of the x-axis resistive quantity, $Z'(1\ \mathrm{Hz})$, are directly related to the number of conductive backbone paths that connect the electrodes.

For the 500 × 500 structure, the shortest (straight-line) single percolating conductive path between the electrodes leads to a backbone resistance of $5 \times 10^5\ \Omega$. Longer conductive paths would lead to larger values, and all 500 minimum-length resistive backbones in parallel would yield 1000 Ω. But such a structure, of nearly vanishing probability, would require the presence of all 500 capacitances in bridging (horizontal) positions, ones with no effect in the dc limit. For x-axis values of less than $5 \times 10^5\ \Omega$, more than one backbone must be present, while for greater values one or more longer than minimum backbone paths connecting the electrodes would be necessary.

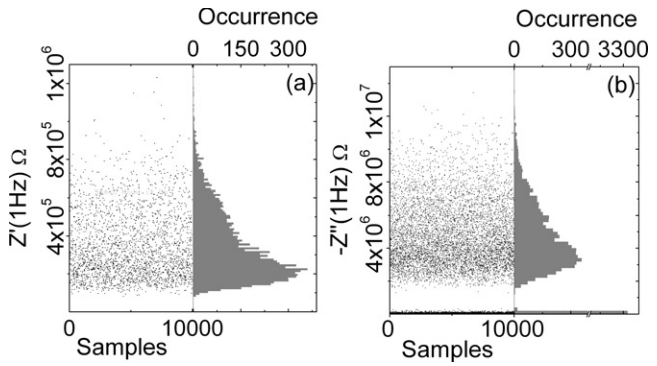

Figure 3. Scattering and distributions of $Z'(1\text{ Hz})$ and $-Z''(1\text{ Hz})$ responses for 10^4 50/50 samples at the 500 × 500 network size. To account in part (b) for both the main distribution and the narrow one at the bottom, the upper right x-axis scale is broken to provide two separate scale sizes.

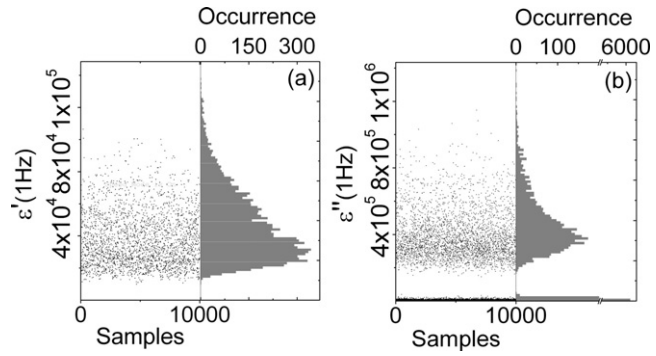

Figure 4. Scattering and distributions of $\varepsilon'(1\text{ Hz})$ and $\varepsilon'(1\text{ Hz})$ responses for 10^4 50/50 samples at the 500 × 500 network size. To account in part (b) for both the main distribution and the narrow one at the bottom, the upper right x-axis scale is broken to provide two separate scale sizes.

Note that the presence of even one capacitance replacing a resistance element in a conducting backbone would render it non-conducting and destroy percolation for that path. Paths with one or more such conductive breaks yield dielectric rather than conductive dispersion. As shown by comparison of the y-axis scales of figures 2(a) and (b), the proportion of samples with dielectric behavior is much greater than conductive ones, and it reflects the dominance of the capacitive effect in the immittance response throughout the whole number of samples. So, we can predict two main behaviors.

(i) Conductive dispersions induced by an integral resistive path leading to a non-zero σ_0. Only for networks of $p < 0.5$ configuration, however, does a high-frequency-limiting σ_∞ quantity also appear.

(ii) Dielectric dispersions that involve either series capacitative elements in a resistive path or the presence of integral capacitive paths. Both types lead to a non-zero static permittivity ε_0 but only those with $p > 0.5$ also include a high-frequency-limiting permittivity ε_∞.

Figure 2(a) shows the presence of two separate distributions of the imaginary part of the impedance. The first one, at the smallest values of $Z''(1\text{ Hz})$, reflects the proportion of the samples with an integral resistive backbone, those leading to conductive dispersion. The second type of distribution is of much broader log-normal character and represents the proportion of samples with a dielectric dispersion caused essentially by the presence of one or more capacitive inclusions in the resistive backbone. These two distributions are separated by a range of improbable values of $Z''(1\text{ Hz})$. The length of the resulting gap depends on the size of the system and increases with the value of L. The minimum value of the real-part impedance results of figure 2(b) also increases with the size of the system and its log-normal distribution correspondingly broadens.

The scattering of the values of the real and imaginary part of the impedance and permittivity is plotted in figures 3 and 4, clearly demonstrating the gap in both quantities. Furthermore, an interesting plot of the phase angle of the admittance is presented in figure 5 and clearly reflects the gap between the

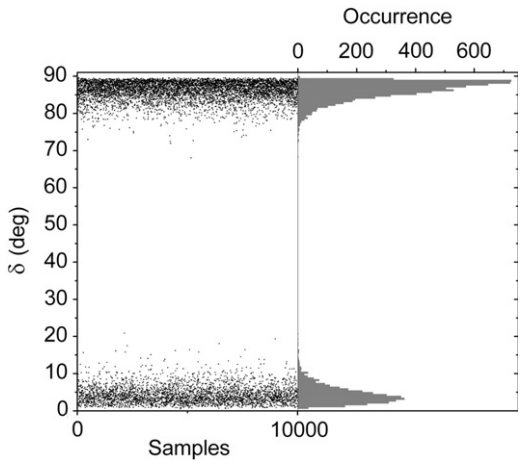

Figure 5. Scattering and distributions of phase angle at 1 Hz for 10^4 50/50 samples at the 500 × 500 network size.

capacitive behavior characterized by $\delta \approx \pi/2$ and the resistive one, by $\delta \approx 0$. This gap is associated with a set of structures of the network that involve improbable and essentially impossible responses and so do not lead to phase values in its range. But the width of the gap does seem to depend on the geometrical structure of the network. Although the system is composed only of capacitive and resistive elements, it allows no intermediate response region but only responses distributed near the exact dc phase values of 0° and 90°. This behavior may be a consequence of the geometry of the network, and we suspect that the gap may be different for more complex geometries than the square network, ones such as triangular, honeycomb, or random.

In figures 6 and 7, distributions of complex resistivity and permittivity at two different frequencies (1 Hz and 10 mHz) are shown for simulations with 10 000 different RC configurations. These results indicate that all the configurations show dc response at these frequencies: conductive and dielectric relaxations are finalized. It is trivial to separate percolating and non-percolating configurations from the imaginary parts of resistivity. Z'', and permittivity, ε''; both yield two different separations, and the results for the two different

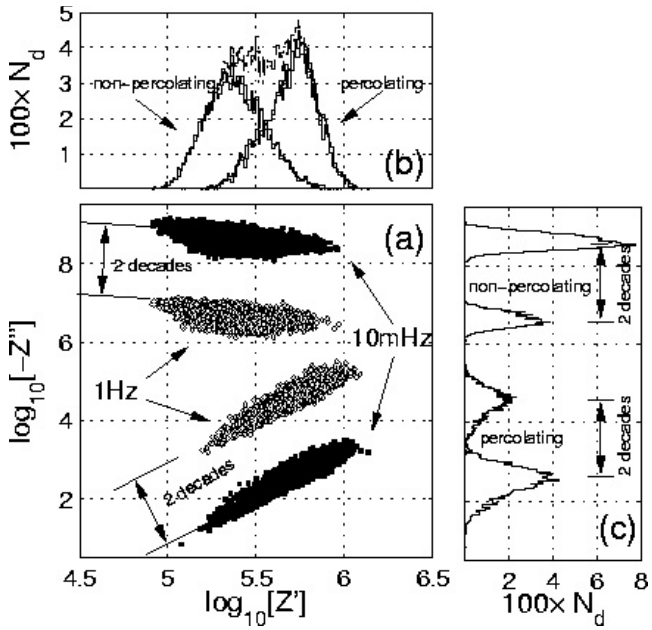

Figure 6. (a) The distribution of the imaginary resistivity $-Z''$ versus the real resistivity Z' for the 500×500 size lattice, calculated from 10 000 different simulations. The simulations were performed at the two frequencies, 1 Hz (open symbols) and 10 mHz (filled symbols). The structures with finite and infinite clusters can be visualized easily: low $-Z''$ means that the structures are less resistive due to percolation. The shift in the $-Z''$ for the two considered frequency cases is due to capacitive impedance, $(\omega\varepsilon')^{-1}$, where ε' is the capacitance of the random structure. (b) The number density of the Z'-distribution of the non-percolating (finite) and percolating (infinite) clusters for the 10 000 cases presented with solid lines and the dashed lines represent the sum of two distributions. Observe that the two frequencies lead to very similar Z' distributions. (c) The number density of the $-Z''$ distribution of the non-percolating (finite) and percolating (infinite) clusters. A clear separation between $-Z''$ distributions is significant in this representation. This splitting occurs only at $p = p_c$ and near the DC limit and depends on the size L and the frequency. It demonstrates the probabilistic character of the geometric percolation: i.e., due to the structure and the content of the backbone not all the samples are conductive at $p = p_c$.

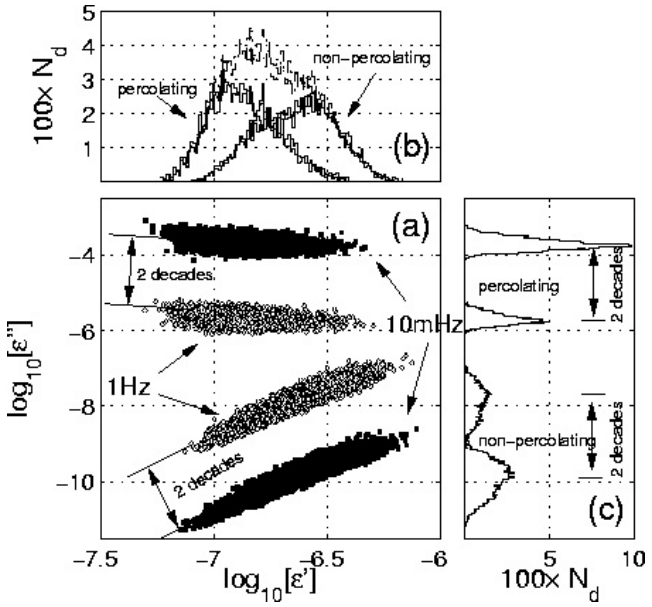

Figure 7. The distribution of the imaginary permittivity ε'' versus the real permittivity ε' for the 500×500 size lattice, calculated from 10 000 different simulations. The simulations are performed at the two frequencies, 1 Hz (open symbols) and 10 mHz (filled symbols). The structures with finite and infinite clusters can be visualized easily: low ε'' means that the structures are less resistive due to percolation. The shift in ε'' for these cases is due to resistive part of the impedance, $(\omega Z')^{-1}$, where Z' is the resistivity of the random structure. (b) The number density ε'—distribution of the non-percolating (finite) and percolating (infinite) clusters for the 10 000 cases presented with solid lines, and the dashed lines represent the sum of finite and infinite clusters. The two frequencies lead to the same ε' distributions. (c) The number density of ε'' distribution of the non-percolating (finite) and percolating (infinite) clusters. A clear splitting occurs only at the p_c value and near the DC limit in the ε'' distributions. This separation, which depends on the size L and the frequency, shows the probabilistic character of the geometric percolation: i.e., due to the structure and the content of the backbone not all of the samples percolate at $p = p_c$.

frequencies have two-decade shifts corresponding to the ratio of the considered frequencies, and dependent on the size of the system as expected.

The results shown in figures 6 and 7 indicate that decreasing the frequency (near dc) tends to separate structural differences more significantly: note especially the two distributions in the imaginary part. A comparison of the current results to a similar study with a small tile structure [33] demonstrates the importance of near dc condition in differentiating between percolating and non-percolating structures.

As the frequency decreases, the distribution of percolating structures tends to shift toward lower Z'' values and the opposite is found for the distribution of non-percolating structures. For the epsilon level, however, these shifts are reversed such that the frequency dependence of the capacitive component contributes more to the total response. For a non-percolating structure as the frequency decreases toward zero we see an increase in the polarization of the dielectric bonds, which leads to lower values of ε'' and higher ones for Z''. On the other hand, percolating structures show lower values of Z'' and higher ε'' ones, due to non-zero dc conduction.

It follows from these results that increasing the frequency tends to bring the two distributions together until they overlap at sufficiently high frequencies. Our results also indicate that not all of the 10 000 samples percolate even when the 50/50 condition is well reached. In fact, the majority of the samples then involve non-percolating behavior, confirming the dominant effect of the dielectric bonds on the structure of the backbone. The real parts of the resistivity, Z', and permittivity, ε', on the other hand yield similar distributions for the two frequencies considered. There is no clear separation between the percolating and non-percolating configurations. However, the percolating configurations result in low dielectric permittivity ε' and high resistivity Z' values, confirming the findings in Tuncer *et al* [34].

The present results emphasize the importance of the content and structure of the percolating backbone in the determination of the nature of the immittance response. The various RRCN at the percolation threshold showed

different dispersions. We thus conclude that these different RRCN combinations had a variety of percolating backbone structures. Considering the nodes–links–blobs model and the self-similar distribution of the resistance blobs, these varieties of percolating backbones should have different fractality and lengths which can affect the properties of the whole system. The effect is not restricted to the static regime but is also present in the dynamic ones where the relaxation process is influenced by the geometrical disposition and the connectivity of the components.

In analogy to real materials, the same effect can be observed by changing the synthesis process of an inhomogeneous material. This process can influence the nucleation growth, segregation, diffusion, and cluster formation. It can thus lead to different structures with diverse fractal dimensions and dispersions that reflect the morphology. It is well known that tuning the electric conductivity and the proportion of the components can enhance the static effective conductivity of the system. Further, tuning the morphology and fractal geometry of the components can provide more control of the physical properties in the dynamic regime.

The dispersions for both states shown in figure 1 demonstrate that the relaxation processes obey a non-exponential law. Such non-Debye behavior involves DRTs that may be used to describe the polarization processes of many disordered systems and can be represented by such models as the DC, KD, K0, and K1 ones described and used in section 3. Another example is the derivation by Nigmatullin *et al* [46] of Davidson–Cole (DC) model [41, 47] response by considering a self-similar relaxation process. They assumed that macroscopic relaxation involved the relaxation of an enormous number of elementary components on the microlevel. The distribution of these components over a fractal geometry led to a fractal distribution of relaxation times. They then obtained the DC model for the complex susceptibility through the analytic derivation of a fractional-order differential equation for the relaxation function. Finally, the DC model exponent was shown to be related to the fractal dimension of the distributed temporal response.

The approach of [46] is reasonable since it is well known that percolating backbones are self-similar and have been treated as fractal objects in different works [2, 24]. The fractal concept has been explicitly applied to microemulsions and their dielectric properties have been investigated by different scientists. For example, Van Dijk *et al* [48] investigated the dielectric properties of microemulsions at the percolation threshold and found scaling behavior in agreement with the predictions of percolation theory. Somewhat later, Clerc and co-authors [2] interpreted Van Dijk's results explicitly in terms of a RC model in a percolating geometry.

Feldman *et al* [49, 50] used the dipole correlation function for microemulsions, one which exhibits non-exponential behavior in the percolation region. To represent experimental correlation-function temporal response of microemulsions they used a sum of two stretched exponentials terms and related their parameters to the structure of the system, reflecting the cooperative behavior of microemulsion droplets near the percolation threshold. Since the dispersive response of a RRCN structure is governed by the electrical current interactions between all of its interconnected elements, one expects that the random distribution of such elements over the network might model the dipole–dipole electrical field interactions or the ion–ion correlations in real disordered materials. In section 3 and in the appendix we explore how well models known to fit dispersed frequency response in such materials actually fit RRCN response for three types of structures with the choices $p = 0.4$, 0.5, and 0.6.

3. Summary of CNLS fitting of individual RRCN data sets for $p = p_c$ and $p \neq p_c$ choices

Many different fitting models have been employed, using the free LEVM CNLS computer program [51], to fit specific 2D RC-square-network data sets in order to find best fitting choices and to best interpret the physics of the responses. Tables A.1 and A.2 of the appendix show representative proportional-weighting fitting results for models that led to the best fits of five data sets, all derived from the responses of 500×500 RC networks. Here we discuss the main conclusions that follow from these fits.

In 1999 Almond and Vainas [10] pointed out a remarkable similarity between the dielectric response of 2D RRCN response and that of the dielectric-level DC model [41], one that has been widely used to fit dielectric materials, conducting polymers, and even a $L = 16$ network of binary dielectric mixtures [33]. In addition, DC response can appear from the presence of self-similar relaxation processes [46], as discussed in section 2. The concave dielectric curves of figure 1(b) are of approximate DC shape, shown by Lindsey and Patterson [47] to be similar to the important dielectric-level Williams–Watts–Kohlrausch model, here designated the KD model and derived from dispersive stretched-exponential temporal response [13, 37–40], widely observed behavior.

Similarly, the concave conducting curves of figure 1(a) are also of approximate Davidson–Cole shape when this model is defined at the impedance level. When the dielectric-level KD model is defined at that level, it is designated the K0 one and is also of approximate impedance-level DC form. Although simple expressions for the frequency-domain responses of the KD and K0 models are unavailable, nevertheless they may be accurately calculated and used for simulation and fitting, as discussed below. Another very important conductive-system model is the K1, related to the K0 by a simple transformation [37–39].

The appropriateness of DC, KD, K0, K1, and other models for fitting RRCN data is demonstrated in detail in the appendix. Note that when the characteristic shape parameter of the DC model, γ, with $0 < \gamma \leqslant 1$, is equal to unity the DC model simplifies to the Debye one, denoted here by DB. The corresponding shape parameters of the KD, K0, and K1 models are β_D, β_0, and β_1, respectively. All these dispersed-response models involve a characteristic relaxation time as well, one that we shall just denote here by τ_0.

There has been no CNLS fitting of 2D RRCN response data with either the DC or KD model thus far, although the DC has been used for approximate fitting of 3D dielectric-level

conductor–insulator composite data [35]. Since the complex-plane results of figure 1 show that concave response curves of DC or KD shape appear for both conductive-system and dielectric-system responses, it is reasonable to fit these models at both the dielectric level (then designated as DCD and KD) and at the impedance one, where they are designated as DC0 and K0. The conductive models are of the same form as the corresponding dielectric ones but involve distributions of resistance-element relaxation times [38, 39]. For simplicity, we shall usually use just the DC and DB designations for both conductive and dielectric-level models and distinguish them by identification of which DRT character they involve. Detailed results of CNLS fitting of RRCN data samples for the $p = 0.4$, 0.5, and 0.6 choices using the DC, KD, DB, K0, and K1 models are presented in the appendix.

The $p = p_c = 0.5$ fits of table A.1 show that although the use of a single fitting model is much inferior to composite models, the single KD one was far superior to the DC one for figure 1(b) dielectric behavior. Interestingly, composite models with two individual ones in parallel or with two in series led to comparable results with, for example, two parallel DC models of dielectric character or series ones of dielectric and conductive character such as the series DCDB combination. Although the fits of table A.1 involve either dominant dielectric or dominant conductive response, the best fits demonstrate for the first time that in either case for each composite model one of the two individual models involves a fractional exponent of value very close to p_c. These results, for both dielectric and conductive situations, confirm the threshold character of the $p = 0.5$ RRCN structures involved and, as well, show that for the 50/50 configuration no high-frequency-limiting ε_∞ and/or ρ_∞ quantities are needed in fitting data for such structures.

The 60/40 and 40/60 fits of table A.2 are of primary dielectric or conductive character, respectively. But, unlike the 50/50 results, the 60/40 ones require the inclusion of a separate non-zero ε_∞ fitting parameter and the 40/60 ones include a non-zero ρ_∞ one. These results indicate the presence of unbroken percolation backbones between the electrodes. Again, composite fitting models are superior to single ones, but it was discovered by CNLS fitting that cutting off the KD (60/40) or K0 (40/60) distribution of relaxation times at a specific minimum τ value, τ_{min}, led to much improved fits in the high-frequency region of the data. This quantity is related to the U cutoff parameter in table A.2 by $\tau_{min} = \tau_0 \exp(U)$, where U is generally negative.

Although separate high-frequency-limiting fitting parameters are needed for the dominantly dielectric 60/40 situation and for the dominantly conductive 40/60 one, as shown in the appendix, cutoff of the KD DRT leads to the additional presence of ρ_∞ response and cutoff of a K0 model DRT correspondingly generates ε_∞ response [52]. Thus, when $p \neq p_c$, the present CNLS data fitting confirms that both types of high-frequency-limiting quantities are intrinsic contributors to the data, are accounted for in the good composite model fits, and both disappear as $p \to p_c$. Further, both the dielectric and conductive 50/50 fittings led to a fractional exponent whose estimated value was very close to p_c. This result was not as interesting, however, as those found on fitting with composite models such as the 60/40 CKDKD composite dielectric model or the 40/60 K0K0R conductive one. They both also led to one part of the model with a fractional exponent again very close to p_c and the other part with fractional exponents of about 0.40 for the 60/40 situation and 0.6 for the 40/60 one, just as one might expect but not previously demonstrated.

The need for a composite model to fit the RRCN dispersive data could arise from the presence of two different fractal processes. The first one could be attributed to the percolating backbone between the electrodes. The second process might represent dispersed clusters surrounding but not connected to the backbone. These processes could be additive depending on whether they are connected in series or in parallel. The two fractal structures are self-similar and would contribute to the response at different levels. Since the fractional power law is directly connected to the fractal dimension of the structure, the two structures would not be too different in terms of fractality. In 1987 Niklasson demonstrated the effects of percolating clusters and the clusters' distribution on the dielectric response by using a fractal scheme [53]. He later further discussed the fractal aspect of dispersive response by connecting fractal structure to dielectric response by means of a Davidson–Cole function [54].

For real materials, one always needs a dipole-rotation ε_∞ free fitting parameter, but only rarely is a ρ_∞ one required. Nevertheless, if the data extend to high enough frequencies, fitting will always require cutoff of model DRTs even when an explicit ρ_∞ parameter is absent. In this respect, RRCN data and its fitting parameters are similar to those of real materials and we can thus learn from such data. Although there is no limit to the smallness of ideal RRCN cutoff parameters, ones which seem to decrease as the size of the network increases, for real materials and networks involving finite-size elements, the finite speed of light will eventually lead to a minimum DRT relaxation-time cutoff value and to a resultant primitive relaxation time, t_c [52, 55, 56]. If the effective speed of light is a limitation, the value of t_c should increase as the separation between electrodes increases.

The CNLS fitting results also led to two other important conclusions. As shown in section A.3 of the appendix, a new duality between fitting models for dielectric and conductive response allows data and a fit for either one to be used to obtain fit results and fit parameters for the other without the need for actual fitting at the other level but only involves a re-interpretation of the meaning of the original fit parameters. This duality nearly doubles the applicability of the fitting results of tables A.1 and A.2 of the appendix.

Finally, in section A.4 it is shown that the present RRCN fitting results involving cutoff are consistent with the Ngai coupling model and with the cutoff model [52–54], both equivalent for real materials in the lower temperature region but only the cutoff one physically appropriate for high temperatures [54]. The coupling model involves a relation between τ_0, τ_e, and τ_c, where τ_e is the relaxation time associated with the Debye response that appears above the cutoff frequency, and the primitive relaxation time τ_c is often taken to be about 2 ps for real materials. Interestingly, RRCN estimates for τ_c were found to be somewhat smaller as well

as somewhat larger than the 2 ps value but still of the same order of magnitude. Thus again we find that the present RRCN behavior is similar to that of real materials and can perhaps help understand which properties of such materials are general and which specific to the material.

Acknowledgment

We greatly appreciate the valuable comments and suggestions of Professor Gunnar A Niklasson.

Appendix. Details of CNLS fitting results

Tables A.1 and A.2 show representative proportional-weighting fitting results for models that led to the best fits of five data sets, all derived from the responses of 500 × 500 RC networks. Although good fits required a composite model with more than one model in series or in parallel, some fits with simpler models are included here to show the progression to a best fitting choice. When exactly 50% of elements of each type are present, the capacitor–resistor number ratio is unity and $p = p_c = 0.5$, the percolation threshold value for a two-dimensional arrangement. For this situation, one might expect to obtain results exactly at the transition from dielectric to conductive behavior. But since the placement positions of the elements are random, a specific realization, such as those considered here, may yield either overall dielectric behavior or overall conductive behavior, as illustrated in table A.1 for rows 1–5 and 6–11, respectively, and in figure 1. In addition to these threshold data sets, rows 1–4 and 5–10 of table A.2 show fits with 60/40 and 40/60 capacitor/resistor ratios, respectively.

A.1. 50/50-structure fit results

The simple DC model fit of table A.1, row 1, which involves only three free parameters, yields the very poor fit value of 12.4% for $100S_F$, the per cent relative standard deviation of the fit residuals. Here, however, the quantity PDRMS, the rms value of the estimated relative standard deviations of the parameters, has an acceptable value of 0.022, indicating adequate estimation of the parameter values. Since both these quality-of-fit measures should be simultaneously as small as possible, the row-1 fit is unsatisfactory. In contrast, the KD fit of row 2 is acceptable and leads to a very well determined estimate of β_D of 0.504, very close to the $p = p_c$ value of exactly 0.5. Nevertheless, this fit can be appreciably improved.

Rows 3–5 involve composite fit models, the first two with models in parallel at the dielectric level and the last one with the models in series. The row-5 results yield not only an excellent fit but also exceedingly well determined parameter estimates with γ_a nearly identical to p_c. Note that here the series Debye model is of resistive rather than dielectric character and involves a fixed γ_b value of unity. Figure A.1 presents both complex dielectric plane and ε'' frequency-response responses for the row 1–5 fits of table A.1. The row 4 and row 5 fit curves are so close to those of the data in both figures A.1(a) and (b) that they are not separately shown. It is clear that although the simple KD fit is much

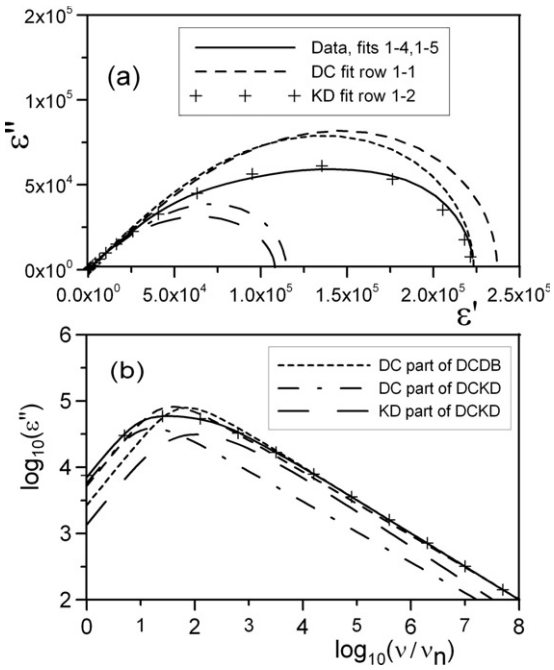

Figure A.1. (a) Complex-plane plot of individual ε response data, fits, and separate parts of composite fitting models for a 50/50 network. (b) Log–log plot of $\varepsilon''(\nu)$ for the same situations as in (a). Here and in table A.2, a designation such as 1–4 refers to the fit listed in the fourth row of table A.1. Here and elsewhere, ν_n is 1 Hz.

superior here to the DC one shown in these figures, the DC model is a crucial part of the best-fit composite models. Also shown are the responses of individual parts of the DCKD and DCDB models.

Rows 6–11 of table A.1, for an overall conductive-response data set at the percolation threshold, again show that a single DC model leads to a poor fit, and parallel composite models are needed to yield better fits. The row 11 parallel combination of an impedance-level DC model and a DC dielectric one seems to be the best of the fits shown and yields a value of γ_a properly near 0.5. Note that for this overall conductive-type data, this value of γ_a is associated with a DC model defined at the resistivity, not dielectric level. Also for the fits of rows 5 and 11 the composite model significantly includes parts defined at both the dielectric level and at the resistivity one.

A.2. 60/40 and 40/60 fit results; effects of cutoff

The present dielectric-dominant 60/40 results of table A.2, rows 1–4, all involve a free capacitance parameter denoted C and listed as ε_∞ in the table. Its inclusion, in parallel with the KD model, is necessary to obtain adequate fits, but no separate ρ_∞ parameter is needed. The existence of non-zero values of ε_∞ demonstrates the presence of one or more dielectric percolation backbones extending from electrode to electrode. Similarly, the conductive-dominant 40/60 results of table A.2, rows 5–10, all involve a free resistance parameter denoted R and listed as ρ_∞ in the table. Its inclusion, in series with the K0 model, is necessary to obtain adequate fits, but no explicit

Table A.1. Results of dielectric-level CNLS fitting of 2D 500 × 500 square-RC-network data sets at the percolation threshold. Data involve dielectric (D), or conductive (C) character, and involve p% capacitors and $(1-p)$% resistors, here equal to 50/50. A composite fit model, such as KDKD (a and b parts), may involve series (S) connection or parallel (P) connection. KX models involve $X =$ D (defined at the dielectric level, E), or $X = 0$ or 1 (both defined at the impedance level, Z). DC denotes the Davidson–Cole response model (expressed at E or Z level) and involving a γ fractional exponent. DB is E or Z type Debye response. The 1 F value in row 5 indicates that the DC model γ_b shape parameter is fixed at 1, leading to Debye response.

#P or S; E or Z	Fit model a part b part	$100S_F$ PDRMS	ε_{0a} or $[\rho_{0a}]$ (Ω)	τ_{0a} (s)	β_{Xa} or γ_a	ε_{0b} or $[\rho_{0b}]$ (Ω)	τ_{0b} (s)	β_{Xb} or γ_b
1 E	DC D 50/50	12.4 0.0216	2.37×10^5	7.34×10^{-3}	0.480	—	—	—
2 E	KD D 50/50	1.92 0.0031	2.22×10^5	2.77×10^{-3}	0.504	—	—	—
3 P E, E	KDKD D 50/50	1.31 0.0147	1.18×10^5	9.83×10^{-4}	0.496	1.05×10^5	6.80×10^{-3}	0.683
4 P E, E	DCKD D 50/50	0.894 0.0251	1.15×10^5	1.76×10^{-2}	0.459	1.08×10^5	1.11×10^{-3}	0.531
5 S E, Z	DCDB D 50/50	0.718 0.0044	2.23×10^5	3.82×10^{-3}	0.501	$[1.57 \times 10^5]$	7.61×10^{-3}	1 F
6 Z	DC C 50/50	4.34 0.0131	$[5.14 \times 10^5]$	2.39×10^{-2}	0.504	—	—	—
7 S Z, Z	K1K0 C 50/50	0.961 0.0312	$[4.42 \times 10^5]$	6.71×10^{-3}	0.690	$[9.11 \times 10^4]$	6.19×10^{-4}	0.502
8 S Z, Z	K0K0 C 50/50	1.47 0.0040	$[4.87 \times 10^5]$	1.10×10^{-2}	0.788	$[4.50 \times 10^4]$	1.89×10^{-4}	0.494
9 P Z, E	K0KD C 50/50	1.27 0.0119	$[5.34 \times 10^5]$	2.32×10^{-3}	0.547	1.61×10^5	2.53×10^{-3}	0.551
10 P Z, E	K0DC C 50/50	1.34 0.0086	$[5.32 \times 10^5]$	3.75×10^{-3}	0.520	1.05×10^5	2.59×10^{-3}	0.516
11 P Z, E	DCDC C 50/50	0.856 0.0235	$[5.33 \times 10^5]$	2.01×10^{-3}	0.509	2.73×10^4	1.32×10^{-3}	0.647

Table A.2. Results of CNLS fitting of 2D 500 × 500 square-RC-network data sets at 60/40 and 40/60 occupation ratios. The 60/40 data set fits were carried out at the E level and the 40/60 ones involved Z-level fits. C is the circuit symbol for ε_∞ and R is that for ρ_∞. Row 7 involves K0 and R in series and the combination in parallel with KD. For rows 8–10 all three K0K0R elements are in series. Row 10 involves a different random data set than do lines 5–9. If $\varepsilon_\infty(\rho_\infty)$ is absent, then $\Delta\varepsilon = \varepsilon_0(\Delta\rho = \rho_0)$.

#P or S; E or Z	Fit model a part b part	$100S_F$ PDRMS	$\Delta\varepsilon_a$ or $[\Delta\rho_a]$ (Ω)	τ_{0a} (s)	β_{Xa} or γ_a	$\Delta\varepsilon_b$ or $[\Delta\rho_b]$ (Ω)	τ_{0b} (s)	β_{Xb} or γ_b	$-U$ cutoff param	ε_∞ or $[\rho_\infty]$ (Ω)
1 E	CKD 60/40	7.31 0.0135	6.61×10^3	2.96×10^{-6}	0.531	—	—	—	—	172
2 E	CKD 60/40	1.07 0.0019	6.47×10^3	2.79×10^{-6}	0.503	—	—	—	8.66	189
3 S E, Z	CKDK1 60/40	0.247 0.0225	6.49×10^3	3.20×10^{-6}	0.528	$[2.63 \times 10^3]$	2.97×10^{-6}	0.457	8.60a	191
4 P E, E	CKDKD 60/40	0.210 0.0162	4.09×10^2	4.36×10^{-7}	0.574	6.09×10^3	3.06×10^{-6}	0.511	8.73b	188
5 S Z, Z	K0R 40/60	7.50 0.0139	$[6.06 \times 10^3]$	3.17×10^{-6}	0.531	—	—	—	—	[153]
6 S Z, Z	K0R 40/60	0.963 0.0017	$[5.93 \times 10^3]$	2.99×10^{-6}	0.503	—	—	—	8.72	[168]
7 P Z, E	K0RKD 40/60	0.536 0.0428	$[5.96 \times 10^3]$	2.95×10^{-6}	0.498	1.68×10^1	9.50×10^{-9}	0.856	8.61a	[177]
8 S Z, Z	K0K0R 40/60	0.131 0.0313	$[4.62 \times 10^3]$	4.35×10^{-6}	0.557	$[1.29 \times 10^3]$	5.42×10^{-7}	0.493	8.59a 7.56b	[168]
9 S Z, Z	K0K0R 40/60	0.185 0.0081	$[3.36 \times 10^3]$	6.15×10^{-6}	0.610	$[2.59 \times 10^3]$	9.11×10^{-7}	0.498	7.40b	[166]
10 S Z, Z	K0K0R 40/60	0.209 0.0080	$[3.38 \times 10^3]$	5.87×10^{-6}	0.593	$[2.51 \times 10^3]$	9.10×10^{-7}	0.503	7.42b	[165]

ε_∞ parameter is needed. Further discussion of the physical meaning of ε_∞ and ρ_∞ for RRCN situations is included below.

Comparison of the 60/40 row-4 results with those of the 40/60 rows 9 and 10 shows that they involve a β value near 0.5 and one near 0.6, with the latter value close to $(1-p)$ for the 40/60 one and to p for the 60/40 one. But for the 60/40 situation both values are those of dielectric KD models, while for the 40/60 one, they both are associated with K0 resistivity-

level models. Both models are of the same form and only differ in the immittance level at which they are defined.

Notice that, unlike the 50/50 results of table A.1, the inclusion of one or more cutoff U free parameters [52, 57–59] leads to greatly improved fits in table A.2. The quantity U is defined for a single KX model by $U = \ln(\tau_{\min}/\tau_0)$, where $\tau_{\min}$ is the cutoff value of the τ distribution of the model and U is generally negative. When it is less than -40 or -50 the resulting cutoff occurs far outside the available frequency range and no estimate of U is possible, the no-cutoff case. The combination of ε_∞ and U, as in the good 60/40 row-2 CKD fit, is far superior to the row-1 result without U. Further, the result of fitting with a KD model without ε_∞ but including U is appreciably worse than even the row-1 one because the combination does not lead to non-zero ε_∞ behavior.

Although the 60/40 data set shows no approach to a ρ_∞ plateau of $\rho'(\nu)$ at high frequencies, and the 40/60 one shows no approach to a plateau of $\varepsilon'(\nu)$ at high frequencies, so one might conclude that both the ε_∞ and ρ_∞ parameters are not both explicitly present in the composite-model results of table A.2, the situation is actually more interesting than one might infer from these results when cutoff is present. It turns out that individual K0 models with cutoff lead to non-zero ε_∞ values and cutoff KD ones correspondingly yield non-zero ρ_∞ ones [57–59].

The reason the effects of ε_∞ and ρ_∞ are not both immediately evident in the 60/40 and 40/60 data sets, and in the composite models of table A.2 that involve cutoff KD and K0 parts, is that the effects of the rest of such composite models obscure the plateaus arising from these individual models. For the 60/40 situation, for example, if the effect of the C parameter of the table A.2, row-4 CKDKD fit is subtracted from the data, a plateau then appears in $\rho'(\nu)$. Since cutoff greatly improves the fits, one may conclude that its generation of ε_∞ and ρ_∞ plateaus is important and that RRCN data for either $p < 0.5$ or $p > 0.5$ actually involves the effects of non-zero values of ρ_∞ or ε_∞ parameters, respectively.

A general expression for the $\varepsilon_\infty = \varepsilon_{C0\infty}$ of the K0 model is $\varepsilon_{C0\infty} = \varepsilon_{Ma}[\langle x^{-1}\rangle_0]^{-1}$, where $\varepsilon_{Ma} \equiv \tau_0\sigma_0/\varepsilon_V$ [57, 60]. The quantity $\langle x^{-1}\rangle_0$ is the mean of the $x^{-1} \equiv (\tau/\tau_0)^{-1}$ relaxation-time distribution and is infinite in the absence of cutoff. For the stretched-exponential temporal response of the K0 model with non-zero $\tau_{\min}$ cutoff, $\langle x^{-1}\rangle_0$ must be expressed in terms of an incomplete gamma function [57], but it is accurately calculated when needed by the LEVM fitting program [51][4]. The above relations show how U and $\varepsilon_{C0\infty}$ are inter-related.

Figure A.2 shows that for the $\varepsilon'(\nu)$ curve of the table A.2, row-9, 40/60 data no non-zero ε_∞ appears. But from the full response of the cutoff K0 part-b model of the composite fitting model, both extrapolation of its results to high frequency and the use of the above expression for $\varepsilon_{C0\infty}$ lead to a value of $\varepsilon_\infty \cong 173.46$. Thus, the high-resolution of accurate complex-nonlinear-least-squares fitting with the LEVM program allows us to demonstrate the presence of a non-zero ε_∞ value for the present 40/60 data. Also note that comparison of the parameter estimates of rows 9 and 10, included to assess statistical variability by using entirely different individual RRCN data sets, shows surprisingly close parameter value agreements and strongly suggests that their β_{0b} estimated values are close approximations to the percolation threshold value of exactly 0.5. Further, both their β_{0a} estimates are properly close to 0.6, the value of the resistive proportion $1 - p$ here.

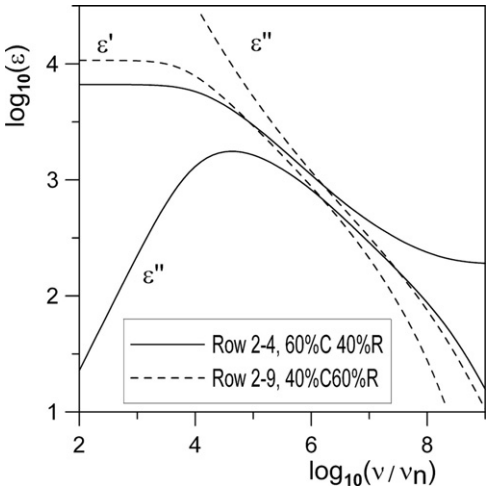

Figure A.2. Log–log plot of $\varepsilon'(\nu)$ and $\varepsilon''(\nu)$ for 60/40 and 40/60 situations.

Next, note that the $\sigma'(\nu)$ high-frequency-limiting power-law exponent values for the conductive-system K1 and K0 models and for the dielectric-system KD models are equal to $1 - \beta_1$, β_0, and $1 - \beta_D$, respectively. Similarly, the equivalent Davidson–Cole model (DC) exponents or log–log slopes are $1 - \gamma_{DC1}$, γ_{DC0}, and $1 - \gamma_{DCD}$, respectively. Here the γ_{DC0} quantities in the table associated with the Z symbol are elements of a conductive-system Davidson–Cole model while the γ_{DCD} shape parameter apply to such a model defined at the dielectric level and identified by E in the table. If S_σ is the slope of the real and imaginary parts at the σ level, then $S_\sigma - 1$ is that of the ε-level parts.

Figure A.2 shows the log–log behaviors of the real and imaginary parts of ε for both the 60/40 and 40/60 situations, and figure A.3 shows that of σ'. We see, as expected, that the figure A.2 row 2–4 ε results show regions of approximate -0.5 slope while the 2–9 ones are near -0.6. For the σ results of figure A.3 the slopes of the full model curves are variable and are shown explicitly in figure A.4. There are hardly any regions of constant slope. The matter is made clearer, however, by the figure A.3 σ' curves of the individual parts of the row 2–4 and row 2–9 fits.

As expected, the row 2–9, 40/60 $K0_a$ slope of 0.61 is close to the value of $1 - p$ for this configuration, and that of the 2–4, 60/40 KD_a one, which reaches its high-frequency limit of $1 - 0.574 = 0.426$ by 10^8 Hz, is also close to its $1 - p$ value. Figure A.3 shows that for the 60/40 configuration the expected slope of the KD_b curve, $1 - 0.511 = 0.489$, is close to the percolation threshold value of 0.5. The actual slope of

[4] The newest WINDOWS version, LEVMW, of the comprehensive LEVM fitting and inversion program, as well as the MS-DOS version, may be downloaded at no cost from http://jrossmacdonald.com. It includes an extensive manual and executable and full source code. More information about LEVM is provided at this website.

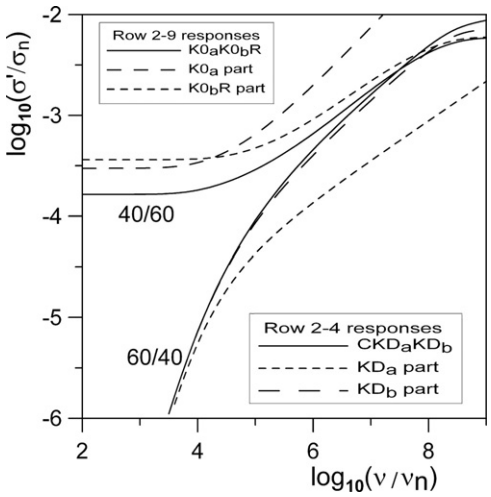

Figure A.3. Log–log plot of $\sigma'(\nu)$ for 60/40 and 40/60 situations. The 'a' and 'b' subscripts designate the left and right parts of a composite model fit listed in a specified row of table A.2.

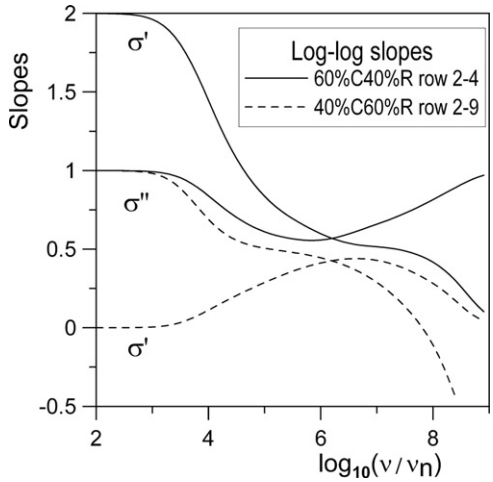

Figure A.4. Log–log slopes of the $\sigma'(\nu)$ and $\sigma''(\nu)$ responses of specified 60/40 and 40/60 situations.

the 40/60 $K0_b$ does not reach its expected value of 0.498 here because there is insufficient length between the low and high-frequency plateaus of this response for the limiting value to be reached. Note that 60/40 full figure A.3 CKD_aKD_b response of row 4 in table A.2, indistinguishable from the data, is much more dominated by its cutoff KD_b part than is the cutoff $K0_b$ part of the $K0_aK0_bR$ model response.

A.3. Duality relations

Consider a new duality transformation that is important for the present data and analysis. Instead of transforming data expressed at, for example, the dielectric level to the resistivity (impedance) level, just re-identify it as applying at the new level, or vice versa! The result is of course different from transforming the original data to the new level. Next consider those fitting models that are of the same form at the two levels even though they involve different DRTs. Such models are the DCD and DC0 (including the Debye model), and the KD and K0. Finally, we ask if a given single or composite model fits well or exactly at one of these levels, what model applies after re-identification of the data at the new level?

Some re-identification transformations or dualities are KD $\leftrightarrow$ CK0, K0 $\leftrightarrow$ KDR, and CKD $\leftrightarrow$ K0R. Note that for CK0 and CKD their elements are in parallel while that of KDR and K0R are in series. Similarly, the dual of the KDKD model with parallel elements is the K0K0 one with its elements in series. Further, the CKD and KDKD composite models apply here to dielectric data, and their duals, the K0R and K0K0, apply to conductive-system resistivity data.

Note that fits of exact KDKD data and fits of the re-interpreted data with its dual K0K0 model involve not only the same number of parameters but ones with exactly the same values of the parameters with the meaning of the parameters correspondingly re-interpreted. Although fit results for the 60/40 CKD model and the 40/60 K0R one are included in table A.2, they there involve different data sets. The present duality relations are different and imply that for each of these composite models there is a dual model involving the same, but re-interpreted data. Thus, for example, the dual of a CDCDDCD model with $p/(1-p)$ would be of the form, DC0DC0R with $(1-p)/p$. Therefore, all fitting results in tables A.1 and A.2 that involve only KD, DCD, K0, and DC0 models have duals. The applicability of the duality transformation is not only consistent with the comparable values of ε_∞ and ρ_∞ present in table A.2, but it also effectively doubles the number of useful results of this table.

A.4. High-frequency coupling and cutoff effects

From the 60/40 row-4 values of U and $\tau_0 = \tau_{0b}$ it follows that $\tau_{min} \cong 4.95 \times 10^{-10}$ s, and from $\nu_{CO} \equiv 1/2\pi\tau_{min}$ one finds $\nu_{CO} \cong 3.22 \times 10^8$ Hz. For comparison, from the 40/60 row-9 values of U and τ_{0b} one obtains the slightly larger τ_{min} value of about 5.58×10^{-10} s. The need for cutoff for these results, but not for those of table A.1, nominally at the percolation threshold, indicates that it is the presence here of percolation backbones, associated with $p \neq 0.5$, that leads to the difference.

As discussed in [54], for conductive-system situations involving K1 model response, the well-known Ngai coupling model (NCM) [52, 55], originally derived for such response, can yield results nearly identical to the simpler and more physically plausible cutoff model [58–60], except at high temperatures where the NCM becomes non-physical. The NCM model invokes a primitive relaxation time or 'crossover' time t_C, usually taken equal to 1 or 2 ps. Since Ngai and co-authors have also applied the NCM to polymeric and small molecular glass formers [55, 61], it is worthwhile to investigate its application to the present dielectric and conductive results as well. The basic NCM relation may then be written as [56, 58]

$$\tau_e/t_c = (\tau_0/t_c)^{\beta_D}, \qquad (1)$$

where τ_e is the characteristic relaxation time of the Debye response that appears at frequencies above the NCM transition and above cutoff for the cutoff model.

For $t_C = 2$ ps, equation (1) yields $\tau_e = 2.89 \times 10^{-9}$ s on using the row-4 KD_b values. But the cutoff model approach of fitting a Debye model to the corresponding high-frequency-limiting data led to $\tau_e = 1.490 \times 10^{-9}$ s. When this value is used in equation (1) to calculate an estimate of t_C, one obtains 0.515 ps, appreciably smaller than 2 ps. In contrast, for the row-9 40/60 $K0_b$ model, equation (1) led to $\tau_e = 1.315 \times 10^{-9}$ s and the cutoff model to 1.634×10^{-9} s. With the latter value, equation (1) then leads to $t_c = 3.08$ ps, nearly six times larger than the 60/40 one. It follows from these results that here $t_c < \tau_{min} < \tau_e$. Although it may only be coincidental that the present RRCN cutoff parameter values are comparable to those found for real materials, the need for DRT cutoff of the response of RC networks demonstrated here, just as for real materials, is of considerable significance. In earlier work, Almond and co-authors [14, 15] have suggested that anomalous power-law dispersion behavior found in a wide range of materials are characteristic of microstructural RC networks. Here we show that the analogy is indeed far more general.

The above results also suggest that decreasing the conductive proportion of the RRCN system decreases the resulting primitive relaxation-time value, perhaps until it and τ_e disappear for 50/50 situations but reappear for $p < 0.5$. In addition, it appears, on comparing the results of figure 4(b) of [10] with those of the present figure A.1, that increasing the total number of network elements also decreases τ_e. Here the value of t_c is associated with percolation and depends on the dielectric–conductive number ratio, but for real dielectric systems Ngai and Capaccioli [62] state that it is determined by the interaction potential. Nevertheless, as we have seen, the cutoff model yields plausible results for the present 2D RRCN structures.

It is worth remarking that in all earlier publications, such as those of Ngai and associates, no complex-least-squares fitting of frequency-response data has been used to estimate NCM or cutoff U and τ_e values directly, as done in the present work and to use the results to estimate t_c values. Such results are currently only made practical by using the LEVM computer program [51]. The present results show that cutoff is needed for all $p \neq 0.5$ values, that a composite fitting model involving two separate dispersive models is required for good fitting of RRCN data, and that for any p value in its full range a pure threshold model with a fractional power-law exponent of 0.5 is always needed as one of the two parts of the composite model.

References

[1] Landauer R 1978 Electrical transport and optical properties of inhomogeneous media *AIP Conf. Proc.* **40** 2–45
[2] Clerc J P, Giraud G, Luck J M and Laugier J M 1990 *Adv. Phys.* **39** 191–309
[3] Bergman D J and Stroud D 1992 *Solid State Phys.* **46** 147–269
[4] Kirkpatrick S 1973 *Rev. Mod. Phys.* **45** 574–88
[5a] Straley J P 1976 *J. Phys. C: Solid State Phys.* **9** 783
[5b] Straley J P 1979 *J. Phys. C: Solid State Phys.* **12** 3711
[5c] Straley J P 1977 *Phys. Rev.* B **15** 5733
[6] Wong P Z 1987 Physics and chemistry of porous media II *AIP Conf. Proc.* **154** 304–18
[7] Sihvola A 1999 *Electromagnetic Mixing Formulas and Applications* (*IEE Electromagnetic Wave Series* vol 47) (Stevenage: Institute of Electrical Engineers)
[8] Tuncer E, Serdyuk Y V and Gubanski S M 2002 *IEEE Trans. Dielectr. Electr. Insul.* **9** 809
[9] Brosseau C and Beroual A 2003 *Prog. Mater. Sci.* **48** 373–456
[10] Almond D P and Vainas B 1999 *J. Phys.: Condens. Matter* **11** 9081–93
[11] Tuncer E 2004 *J. Phys. D: Appl. Phys.* **37** 334
[12] Tuncer E 2005 *J. Phys. D: Appl. Phys.* **38** 223
[13] Macdonald J R 2000 *Solid State Ion.* **133** 79
[14] Almond D P and Bowen C R 2004 *Phys. Rev. Lett.* **92** 157601
[15] Bouamrane R and Almond D P 2003 *J. Phys.: Condens. Matter* **15** 4089–100
[16] Almond D P, Bowen C R and Rees D A S 2006 *J. Phys. D: Appl. Phys.* **39** 1295–304
[17] Roling B, Happe A, Funke K and Ingram M D 1997 *Phys. Rev. Lett.* **78** 2160–3
[18] Kuanr B K and Srivastava G P 1994 *J. Appl. Phys.* **75** 6115–7
[19] Rozanski S A, Kremer F, Köberle P and Laschewsky A 1995 *Macromol. Chem. Phys.* **196** 877–90
[20] Dyre J C 1988 *J. Appl. Phys.* **64** 2456–68
[21] Dyre J C 1993 *Phys. Rev.* B **48** 12511–26
[22] Dyre J C 1994 *Phys. Rev.* B **49** 11709–20
Dyre J C 1994 *Phys. Rev.* B **50** 9692(E)
[23] Dyre J C and Schrøder T B 2000 *Rev. Mod. Phys.* **72** 873–92
[24] Efros A L and Shklovskii B I 1976 *Phys. Status Solidi* b **76** 475
[25] Bergman D J and Imry Y 1977 *Phys. Rev. Lett.* **39** 1222
[26] Stroud D and Bergman D J 1982 *Phys. Rev.* B **25** 2061
[27] Gefen Y, Aharony Q and Alexander S 1983 *Phys. Rev. Lett.* **50** 77
[28] Stauffer D and Aharony A 1994 *Introduction to Percolation Theory* 2nd edn (London: Taylor and Francis)
[29] Coverdale R T, Jennings H M and Garboczi E J 1995 *Comput. Mater. Sci.* **3** 465
[30] Frank D J and Lobb C J 1988 *Phys. Rev.* B **37** 302
[31] Lobb C J and Lobb D J 1984 *Phys. Rev.* B **30** 4090
[32] Tuncer E, Gubanski S M and Nettelblad B 2001 *J. Appl. Phys.* **89** 8092–100
[33] Tuncer E, Nettelblad B and Gubanski S M 2002 *J. Appl. Phys.* **92** 4612–24
[34] Tuncer E, Gubanski S M and Nettelblad B 2002 *J. Electrost.* **56** 449
[35] Calame J P 2003 *J. Appl. Phys.* **94** 5945
[36] Lichtenecker K 1926 *Z. Phys.* **27** 115
[37] Macdonald J R 2002 *J. Chem. Phys.* **116** 3401
[38] Macdonald J R 2005 *Phys. Rev.* B **71** 184307
[39] Macdonald J R 2006 *J. Phys.: Condens. Matter* **18** 629 The word 'imaginary' on the third line of p 643 should be replaced by 'real'. On p 640, next to the bottom line, replace $\rho_0\varepsilon_{D\infty}$ by $\rho_0\varepsilon_V\varepsilon_{D\infty}$
[40] Macdonald J R and Tuncer E 2007 *J. Electroanal. Chem.* **602** 255
[41] Davidson D W and Cole R H 1951 *J. Chem. Phys.* **19** 1484
[42] Skal A S and Shklovskii B I 1974 *Fiz. Tekh. Poluprov.* **8** 1586
Skal A S and Shklovskii B I 1975 *Sov. Phys.—Semicond.* **8** 1029 (Engl. Transl.)
[43] De Gennes P G 1976 *J. Physique Lett.* **37** L1–2
[44] Straley J P 1982 *J. Phys. C: Solid State Phys.* **15** 2333–41
Straley J P 1982 *J. Phys. C: Solid State Phys.* **15** 2343–6
[45] Lin C R, Chen Y C and Chang C Y 2001 *Macromol. Theory Simul.* **10** 219–24
[46] Nigmatullin R and Ryabov Ya E 1997 *Phys. Solid State* **39** 87
[47] Lindsey C P and Patterson G D 1980 *J. Chem. Phys.* **73** 3348
[48] Van Dijk M A, Casteleijn G, Joosten J G H and Levine Y K 1986 *J. Chem. Phys.* **85** 626
[49] Feldman Y, Kozlovich N, Nir I and Garti N 1995 *Phys. Rev.* E **51** 478

[50] Feldman Y, Kozlovich N, Alexandrov Y, Nigmatullin R and Ryabov Y 1996 *Phys. Rev.* E **54** 5420
[51] Macdonald J R and Potter L D Jr 1987 *Solid State Ion.* **23** 61
Macdonald J R 2000 *J. Comput. Phys.* **157** 280
[52] Macdonald J R 2002 *Solid State Ion.* **150** 263–79
[53] Niklasson G A 1987 *J. Appl. Phys.* **62** R1
[54] Niklasson G A 1993 *J. Phys.: Condens. Matter* **5** 4233
[55] Ngai K L 1998 *Phil. Mag.* B **77** 187
[56] Macdonald J R 2005 *Solid State Ion.* **176** 1961
[57] Macdonald J R 1996 *J. Non-Cryst. Solids* **197** 83
Macdonald J R 1996 *J. Non-Cryst. Solids* **204** 309 (erratum)
In addition, in equation (A2) G_D should be G_{CD}
[58] Macdonald J R 1998 *J. Appl. Phys.* **84** 812
[59] Macdonald J R 2000 *Inverse Problems* **16** 1561
[60] Macdonald J R 2001 *J. Appl. Phys.* **90** 153
[61] Ngai K L, Casalini R, Capaccioli S, Paluch M and Rowland C M 2005 *J. Phys. Chem.* B **109** 17356
[62] Ngai K L and Capaccioli S 2007 *J. Phys.: Condens. Matter* **19** 205114